JOURNAL OF PROPULSION AND POWER
Vol. 25, No. 2, March–April 2009

Langmuir Probe Studies of Magnetic Confinement in an Ion Thruster Discharge Plasma

Anita Sengupta,* Dan M. Goebel,† and Allison G. Owens‡
Jet Propulsion Laboratory, California Institute of Technology, Pasadena, California 91109

DOI: 10.2514/1.36547

Magnetic confinement studies on a 30-cm-diameter ion thruster were performed to determine the dependence of plasma confinement and uniformity on the ring-cusp magnetic field. Four primary cases were investigated to determine the effects of an additional magnetic cusp, increasing the strength of the highest value closed magnetic contour line, and varying the magnetic field free volume. A laboratory model NASA Solar Electric Propulsion Technology Application Readiness engine was modified to investigate three- and four-ring-cusp geometries. Electrical parameters and langmuir probe sweeps in the discharge chamber were used to measure the performance of each configuration. Increasing the strength of the closed magnetic contour line reduces ion loss to the anode, resulting in a reduction in discharge power for a given beam current. Similarly, increasing the magnetic field free volume in the near-grid region improves plasma uniformity, removing the on-axis current density peak responsible for accelerator grid erosion. The enhanced magnetic circuit geometries investigated resulted in a 20% reduction in discharge loss and discharge current at the TH15 (2.3 kW) throttle point, with similar gains over the full throttle range. The reduction in discharge power and peak current density can significantly increase the total throughout per engine by limiting wear mechanisms that limit thruster life.

Nomenclature

A_p	=	probe area
e	=	electron charge
$I_{\text{sati},e}$	=	saturation current (ion, electron)
J_B	=	beam current
J_D	=	discharge current
j_i	=	ion current density
k	=	Boltzmann constant
m_e	=	electron mass
n_e	=	electron density
T_e	=	electron temperature
V_B	=	beam voltage
V_D	=	discharge voltage
V_f	=	floating potential
V_p	=	plasma potential
ε_B	=	discharge loss
η_{tot}	=	total efficiency

I. Introduction

ION engines offer the potential for orders of magnitude specific impulse improvement over traditional chemical propulsion systems, resulting in shorter trip times, lower propellant mass, and reduced launch vehicle costs [1,2]. In spite of the tremendous advantages the technology offers, the actual use of ion thruster technology on NASA science missions has been limited, due in part to electrical inefficiencies and reliability/lifetime issues [3,4]. The inefficiencies of the state-of-the-art NASA Solar Electric Propulsion Technology Application Readiness (NSTAR) ion engine are related to the production and confinement of the discharge plasma in the engine's discharge (ionization) chamber. In the current configuration, for every 14.5 A of electron current generated by the discharge hollow cathode, only 1.76 A of ions are actually extracted through the optics assembly to produce thrust. This is largely due to direct loss of ions to the anode walls, where they recombine with the surface. Discharge loss is typically used to define the energy cost to produce beam ions. It is defined as the ratio of the discharge power to beam current. A reduction in discharge loss results in a decrease in discharge current and cathode temperature, which can significantly improve the cathode life, as shown in [5]. For example, a 20% reduction in cathode current results in a 45% increase in cathode life for the NSTAR TH15 throttle point [6,7]. Additionally, reducing the central peak current density of beam ions by improving radial plasma uniformity can increase total propellant throughput, as grid life is limited by accelerator grid erosion, which is linearly proportional to beam current density [8].

The objective of this study was to use a combination of analytical models and experimental plasma property measurements to provide physical insight into the production and confinement of the discharge plasma [9,10]. The measurements included bulk electrical parameters to establish the gross discharge loss for each configuration evaluated and langmuir probe traces to map the plasma structure. This insight can be used to improve thruster performance and lifetime by reducing the discharge loss and improving the plasma uniformity.

II. Experimental Apparatus

The experiments were performed on a laboratory model NSTAR engine, referred to as the NKO1 thruster. The NKO1 engine and flight NSTAR engine are functionally identical, as reported in [11]. The engine tests were performed in a 3-m-diam by 10-m-long vacuum chamber with 1×10^{-5} Pa base pressure and 5×10^{-4} Pa at the NSTAR full-power flow rates. A flightlike propellant-feed system and laboratory power supplies with similar capabilities to the Deep Space One flight power-processing unit were also used to run the NKO1 engine [12]. The NKO1 engine was configured to allow the translation of up to seven single flat-disk langmuir probes, providing radial plasma parameter profiles from the anode wall to

Presented as Paper 4069 at the 41st AIAA/ASME/SAE/ASEE Joint Propulsion Conference & Exhibit, Tucson, Arizona, 10–13 July 2005; received 9 January 2008; revision received 24 September 2008; accepted for publication 2 November 2008.

*Senior Engineer, Systems Engineering, 4800 Oak Grove Drive, Mail Stop 301-490. AIAA Senior Member.

†Principal Scientist, Propulsion and Materials Engineering, 4800 Oak Grove Drive, Mail Stop 125-109. AIAA Associate Fellow.

‡Senior Technician, Propulsion and Materials Engineering, 4800 Oak Grove Drive, Mail Stop 125-109.

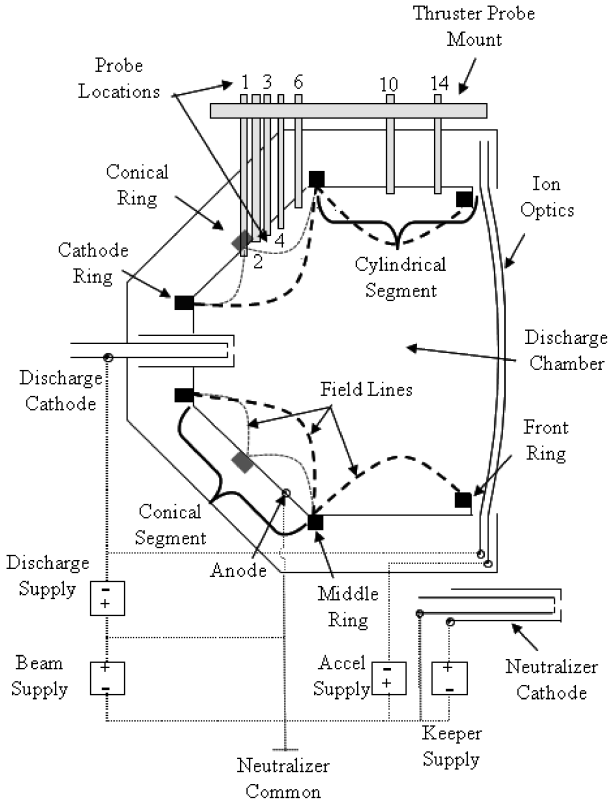

Fig. 1 Thruster schematic indicating electrical connections, functional components, and probe locations. Permanent magnet ring and associating field line in a lighter shade. Probe locations are numbered in centimeters downstream of the discharge cathode.

just past the thruster centerline for both the cylindrical and conical chamber regions, as shown in Figs. 1 and 2. Seven 0.75-cm-diam holes were cut into the anode wall to allow the translation of various probes. The probe locations provided a spatially resolved discharge plasma characterization, from 1 to 14 cm downstream of the discharge cathode keeper in the axial direction. Higher spatial resolution was obtained in the conical region as density and potential gradients are known to be highest in the vicinity of the cathode [13]. The conical region of the chamber extends from 1 to 6 cm downstream of the keeper and the cylindrical region from 10 to 14 cm. The 14 cm location is just upstream of the screen grid and is used to determine the representative beam profile by biasing the probe −25 V negative of cathode common to collect ions. The probes were inserted into and retracted from the discharge chamber by linear translation stage with a maximum speed of 50.8 cm/s. Alignment and insertion into the engine were accomplished by a probe mount, which housed each probe in a stainless steel collar

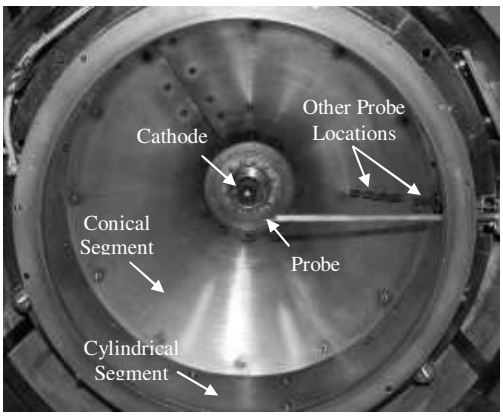

Fig. 2 Langmuir probe as seen from inside the discharge chamber with the optics assembly removed. The 14 cm location langmuir probe is shown translated to the centerline position.

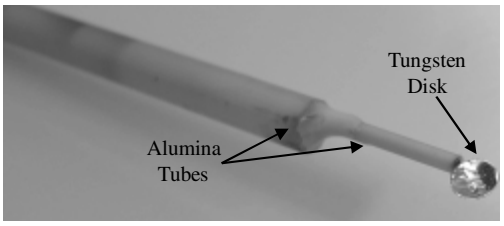

Fig. 3 Flat-disk langmuir single probe.

inserted into the anode wall that protruded up to 0.76 cm into the discharge chamber (Fig. 2) [9].

Flat-plate single langmuir probes were used to eliminate the effect of radial sheath expansion that prevented electron saturation of cylindrical probing in the low density region of the discharge chamber studied previously [9,10]. As the aspect ratio of the disk is 100, end effects are assumed to be negligible. Each probe consists of a 0.4 ± 0.1-cm-diam tungsten disk (0.126 ± 0.007 cm^2) spot welded to a 0.05 ± 0.01-cm-diam Ta wire that was fed through a single bore alumina tube with a 0.2 cm outer diameter and then inserted into a single bore ceramic tube with a 0.48 cm outer diameter (Fig. 3). This dual-ceramic, necked down configuration is chosen to minimize perturbations due to insertion of a large insulating surface into the plasma.

A bipolar power supply was used to bias the langmuir probes ±50 V with respect to cathode common. The voltage waveform was a sawtooth ramp, cycled at 10–100 Hz for 1–3 s. The bias supply was placed in series with the probe and cathode common (discharge supply common), and allowed to float at the thruster potential with respect to ground. The current through each probe was measured across a 1-Ω current shunt to generate current-voltage characteristics. For ion saturation sweeps, a 100 Ω current shunt was used to amplify the signal. The voltage output from the shunt was conditioned using a low-pass resistor-capacitor filter circuit.

III. Probe Data Reduction

Langmuir probes are commonly used to spatially resolve plasma parameters in low-temperature plasmas. Langmuir probes are electrostatic devices that make use of debye shielding to measure collected current of charged particles to a biased object inserted into a plasma. The langmuir probes used in this study are planar electrodes. The current to the probe is measured as a function of the applied bias voltage generating a current-voltage characteristic for a particular location within the ion thruster plasma. As the langmuir probe surface is cold relative to the plasma temperature, it collects charge carriers in accordance with its potential relative to the plasma potential. For large positive potentials relative to the plasma potential, ions can be assumed to be repelled and the current saturates with electrons, defining the plasma potential. Similarly, for large negative potentials, electrons are assumed to be repelled and the measured current is defined as the ion saturation current from which the ion current density can be obtained. A representative langmuir probe trace from the study can be found in [9].

A. Plasma Parameter Determination

In the ion thruster discharge plasma, the electrons are assumed to follow the Maxwell–Boltzmann law: a plasma in thermal equilibrium. In a Maxwellian plasma, the electron-retarding region of the probe trace is proportional to the Gaussian distribution at the electron temperature [14]. Therefore, an exponential curve fit can be to used to obtain the associated plasma electron temperature T_e. It is true that emission of primary electrons from the hollow cathode violates the assumption of a pure Maxwellian plasma, but as they comprise less than 10% of the total electron population and are primarily located in the cathode plume, the error introduced is viewed as acceptable for the purposes of analyzing plasma parameter data, in the context of understanding the physics of plasma confinement.

The plasma potential was determined from the first derivative of the probe trace using the technique in [15]. The first derivative method was chosen for improved accuracy as it can be applied to any type of electron distribution, essentially eliminating curve fitting errors inherent to the semilog method [14].

Electron number density was determined from the electron temperature and electron saturation current measurements, both of which were obtained from the current-voltage traces by the method in [16], as shown here:

$$n_e = \frac{4I_{\text{sat}}}{A_p e\sqrt{8kT_e/\pi m_e}} \tag{1}$$

Ion saturation current measurements were made by biasing each langmuir probe 25 V negative of cathode common potential, to repel all electrons and collect only ions. The ion current density can be calculated as follows:

$$j_i = \frac{I_{\text{sat},i}}{A_p} \tag{2}$$

B. Uncertainty Analysis

Uncertainties in measured parameters are shown in Table 1. Experimental error sources included probe disk diameter, probe current, ion saturation current, bias voltage, and bulk thruster electrical parameters. The largest error in the probe analysis was due to the primary electron population, which introduced error into the calculation of T_e, a result of deviation from a Maxwellian plasma. Without measurement of the electron energy distribution function, the primary electron component to the saturation current cannot be delineated. This error manifests in the exponential fitting process. The fitting error is driven by the range over which to fit the exponential region on the current-voltage probe trace. All fits were achieved with a residue or R-squared value in excess of 0.9, corresponding to 200–500 points on the current-voltage trace. Sensitivity analysis showed that, within this fitting residue, the electron temperature varied by up to $\pm 0.5T_e$. On a 4 eV electron temperature, this is on the order of 25% absolute error. The electron density uncertainty is an rss of the Maxwellian fitting error from T_e and the relevant experimental measurement uncertainties using the technique in [17]. Plasma potential uncertainty is an rss of experimental measurement uncertainties and the error in the forward difference method used to compute the first derivative of the probe current.

IV. Experimental Results

A. Summary of Experimental Studies

Bulk performance and plasma parameter measurements for four separate thruster magnetic field configurations were investigated to parametrically determine the individual effects of 1) adding an additional magnetic cusp, 2) increasing the gauss level of the highest value closed contour line (closed throughout the chamber), and 3) varying the magnetic field geometry with respect to the anode wall

Table 1 Summary of measurement uncertainty

Uncertainty parameter	Uncertainty (±)
Probe current, mA	1
Ion saturation current, mA	0.01
Bias voltage, V	0.1
Probe diameter, cm	0.1
Discharge current, A	0.1
Beam current, A	0.1
Screen voltage, V	1
Accel voltage, V	1
Main flow, sccm	0.7
Cathode flow, sccm	0.1
Neutralizer flow, sccm	0.1
Neutralizer current	0.1
Electron temperature, eV	0.5

Table 2 Summary of NSTAR engine tests

Version	Number of magnet rings	Contour line closure, G
V1 (nominal)	3	20
V2	4	30
V3	4	50
V4	3	50

(Table 2). For each of these cases, a two-dimensional map of the magnetic field was computed with a magnetostatic solver code. The test sequence was to retrofit NKO1 with the new magnetic circuit, measure the individual cusp magnetic field strengths with a gauss meter, and then install the engine in the test facility for experimentation. The goal of the magnetic studies was to determine the dependence of plasma confinement and plasma uniformity on the strength and shape of the imposed ring-cusp magnetic field.

B. Nominal NASA Solar Electric Propulsion Application Readiness Results: Configuration V1

1. *Overall Performance*

Table 3 summarizes the performance of the nominal configuration for full-power (TH15), half-power (TH8), and minimum-power (TH0) operation. Table 4 gives the corresponding NSTAR throttle table operating parameters for these points. Figure 4 shows two-dimensional plots of lines of constant magnetic strength and the magnetic field lines. The nominal thruster configuration closes the 20 G contour line, resulting in a field free volume in the cylindrical segment that is significantly smaller than the physical volume.

2. *Plasma Profiles*

Six flat-disk probes were used in the investigation of the nominal thruster configuration. Figures 5–7 present radial variation in n_e, T_e, and V_p for each axial probe location at the TH15 operating point. Electron number density data are shown from the anode wall to just past the centerline, to illustrate the symmetry and peaked nature of the plasma. T_e and V_p were only measured up to the thruster centerline, as passage of the alumina tubes in front of the cathode tended to disturb its operation.

In the conical region, n_e was found to be peaked on the centerline at a maximum of 1×10^{12} cm^{-3}, 1 cm downstream of the cathode, and decreased rapidly in the radial direction to a minimum of 4×10^{10} cm^{-3} near the anode wall, consistent with other research in the field [13,18]. This structure is consistent with a high-density cathode plume typical of hollow-cathode discharge plasma. In the cylindrical region of the discharge chamber, radial variation in density was not as peaked and varied radially from 4×10^{11} cm^{-3} at the center to 1×10^{11} cm^{-3} at the anode wall. Density gradients in both the radial and axial directions decreased in magnitude with distance from the cathode. In Fig. 6, the radial variation in T_e was similarly peaked. In the conical segment, it spanned from a maximum of 5.5 eV on the centerline to a minimum of 1.5 eV at the anode wall. Radial variation in the cylindrical segment spanned 4.75–3 eV, with the maximum on the centerline and minimum at the anode wall. As shown in Fig. 7, plasma potential was highly depressed on axis from 2 to 14 cm downstream of the cathode. The depression is believed to be due to a high concentration of primary electrons constrained to the centerline. The concentration of negative charge on the centerline then tends to depress the potential.

Table 3 Nominal (V1) performance

Discharge parameter	NKO1 (V1) TH15	TH8	TH0
J_B, A	1.76	1.10	0.51
J_D, V	14.8	8.3	5.3
V_D, V	24.65	26.2	25.70
ε_b, V	207.3	198.3	267.1
η_{tot}	0.609	0.603	0.391

Table 4 Subset of the NSTAR throttle table [12]

NSTAR throttle level	Nominal thruster power, kW	Beam supply voltage, V	Beam current, A	Accelerator grid voltage, V	Neutralizer keeper current, A	Main flow, sccm	Discharge cathode flow, sccm	Neutralizer cathode flow, sccm
TH0	0.52	650	0.51	−150	2.0	5.98	2.47	2.40
TH8	1.46	1100	1.1	−180	1.5	14.41	2.47	2.40
TH15	2.33	1100	1.76	−180	1.5	23.43	3.70	3.60

Therefore, a higher density of primaries on axis will result in a deeper depression of the plasma potential. This on-axis potential depression is consistent with the results of other researchers [13,19]. Moving axially from the cathode exit, the primary density decreases and the plasma potential increases. Axial variation in this region was from 21 to 26.5 V, increasing in the downstream direction. The plasma potential, 1 cm downstream of the cathode exit, exhibited a large increase going radially from the centerline to 1 cm from the centerline, from 21 to 23 V. From 2–12 cm radially, the potential increases monotonically to 24 V. A similar radial profile was measured for the 2 and 3 cm probes, with a centerline potential of 21 V, increasing to 24 V with radial distance from the centerline. There was little radial variation in the cylindrical segment, with the exception of the peak on the centerline. Similar to the electron temperature and density, the gradient in radial variation decreased in the downstream direction, consistent with a more uniform plasma with distance from the cathode.

Variation in ion current density was also measured throughout the discharge chamber. Although not shown, ion saturation current density profiles were obtained in the same radial and axial locations as the electron data. Ion current density was highly peaked on axis in the conical section of the discharge chamber, suggesting that most of the ionization in the nominal configuration occurs within the cathode plume in the vicinity of the cathode. With increasing distance from the cathode, the j_i became more uniform. It is also important to note that n_i was within 10% of the measured electron density for all probe traces investigated, confirming that ions are electrostatically confined by the plasma electrons.

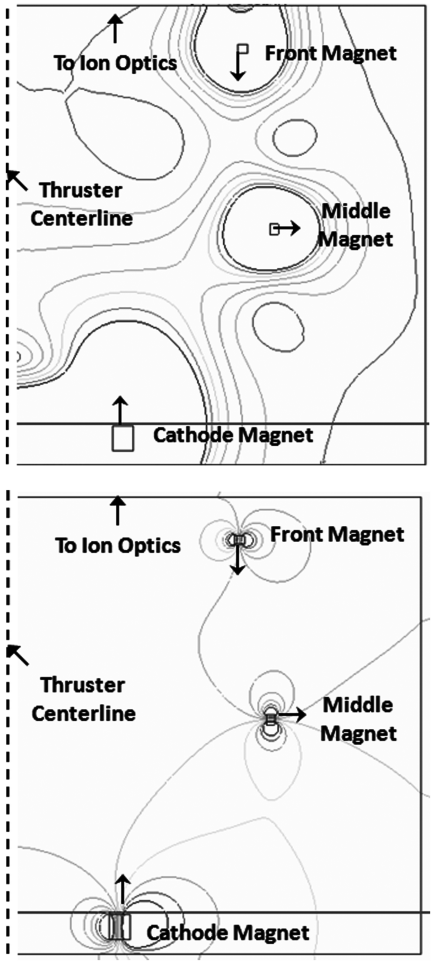

Fig. 4 Two-dimensional axis-symmetric simulation of (top) magnetic field lines and (bottom) contours of constant magnetic field of the V1 configuration. Arrows next to each magnet indicate the direction of magnetization. Thruster centerline was the axis of symmetry for the simulation.

C. Enhanced Four-Ring-Cusp NASA Solar Electric Propulsion Application Readiness: Configuration V2

1. Overall Performance

Configuration V2 is a four-ring-cusp modified NSTAR engine. In this configuration, a ring of magnets was added to the center of the conical section of NKO1, with the direction of magnetization into the discharge chamber, normal to the magnet surface. To retain the alternating polarity cusp design, the cathode ring polarity was reversed and the middle and front magnet rings left unchanged. A thin steel shim was placed in the interior of the chamber to aid in the

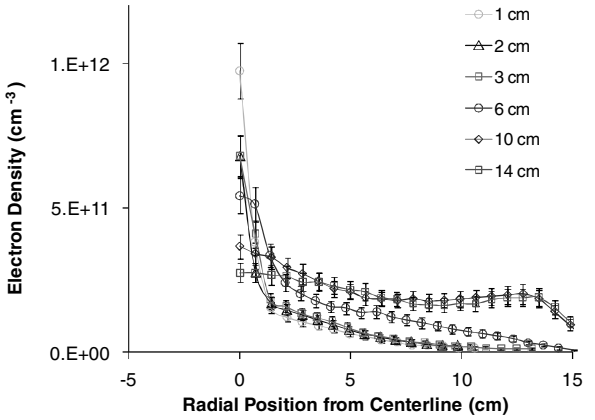

Fig. 5 Electron number density radial profiles at TH15 for the V1 configuration.

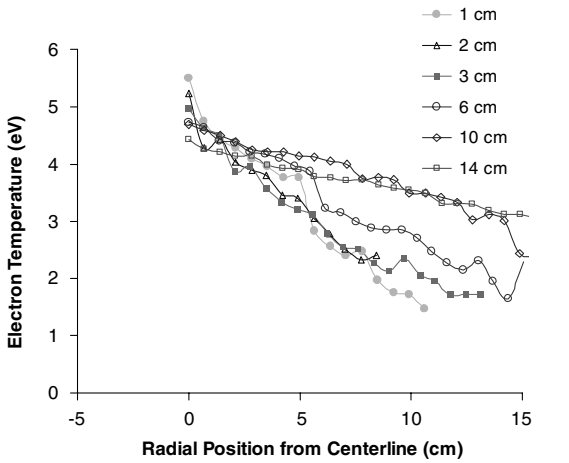

Fig. 6 Electron temperature radial profiles at TH15 for the V1 configuration. Measurement uncertainty is ±0.5 eV for all traces.

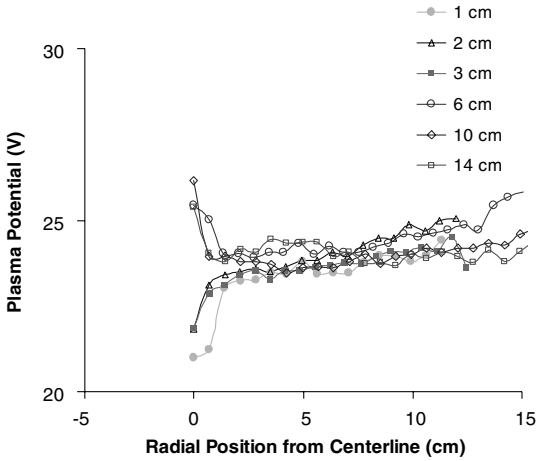

Fig. 7 Plasma potential radial profiles at TH15 for the V1 configuration. Measurement uncertainty is ±0.5 eV for all traces.

retention of magnets to the cone section. Although this aided in magnet insertion, the ferrous material resulted in a significant lowering of the cusp strength, reducing its effectiveness at confining electrons. Figure 8 presents the two-dimensional magnetic contour and field lines for the V2 configuration. Although this configuration closes the 30 G contour throughout the chamber and increases the field free volume in the cylindrical segment, it does not result in a noticeable performance change over the nominal configuration

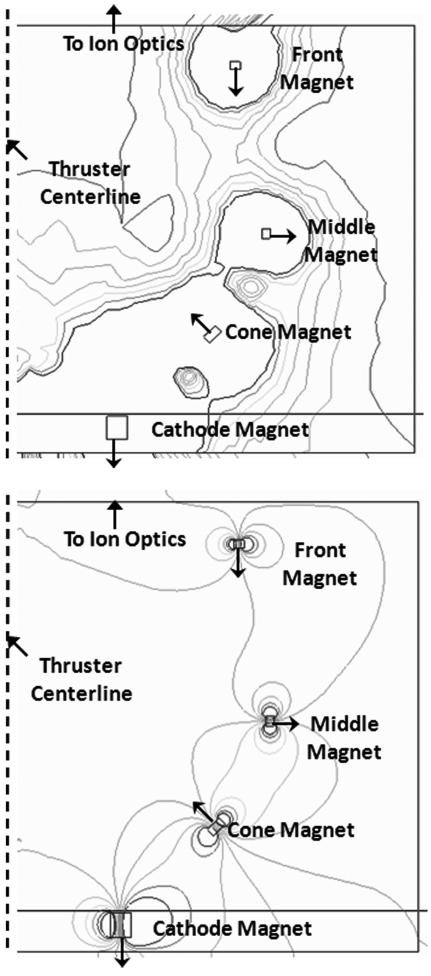

Fig. 8 Two-dimensional axis-symmetric simulation of (top) magnetic field lines and (bottom) contours of constant magnetic field of the V2 configuration. Arrows next to each magnet indicate the direction of magnetization. Thruster centerline was the axis of symmetry for the simulation.

Table 5 Enhanced four-ring-cusp (V2) performance

Discharge parameter	NKO (V2) TH15	TH8	TH0
J_B, A	1.76	1.10	0.51
J_D, V	14.3	8.5	5.3
V_D, V	24.7	25.1	25.5
ε_b, V	201.4	194.5	265.0
η_{tot}	0.612	0.605	0.392

(Table 5). As in the nominal case, TH15 operation is defined by the set points in the NSTAR throttle table. Therefore, changes in performance for V2 versus V1 are limited to changes in the discharge current and voltage required to produce and extract 1.76 A of beam current through the optics. This can be attributed to the weak cusp strength of the new conical magnet ring because of the steel shim used to retain the magnets. A ferrous material shunts magnetic field lines and, therefore, use of the shim reduced the surface magnetic field strength. Measurement of the cusp strength with a gauss meter revealed it was only 820 G, insufficient to prevent measurable primary electron loss to the cusp. The shim was subsequently removed for V3 and the cusp strength increased to 1800 G. V2 testing was made with the shim in place.

2. *Plasma Profiles*

Figures 9 and 10 present the radial variation in n_i and T_e for each axial probe location at the TH15 operating point. All probe traces were made from the anode wall to just past the thruster centerline, identical to the nominal case. In the conical region of the discharge chamber, the radial variation in electron density had a primary peak on the centerline, as well as a secondary peak off axis. The primary peak on the centerline was due to the cathode plasma plume and had a maximum value of 8.75×10^{11} cm^{-3}, as measured 1 cm downstream of the cathode. The secondary peak was caused by the addition of the conical magnet ring, causing electrons to leave the centerline axis and to travel along the new field lines to the conical magnetic cusp. The maximum number density in the secondary peak was 1.5×10^{11} cm^{-3}, as measured 9 cm radially from the centerline, by the probe 4 cm axially downstream of the cathode. The radial variation of electron density in the cylindrical region of the plasma was relatively flat, confirming that a field free volume in necessary for increased plasma uniformity. Electron density varied from a maximum of 2×10^{11} cm^{-3} on the centerline to 1.5×10^{11} cm^{-3} near the anode wall in the cylindrical segment. The radial variation in T_e in the conical segment was peaked on axis (5.2 eV), with an additional off-axis peak (4.8 eV) corresponding to the electron density peaks described previously. T_e reached a minimum of 2 eV near the anode wall in the conical segment. Radial variation in the cylindrical segment was less peaked and spanned 4.5–3 eV, with the maximum on the centerline and minimum at the anode wall.

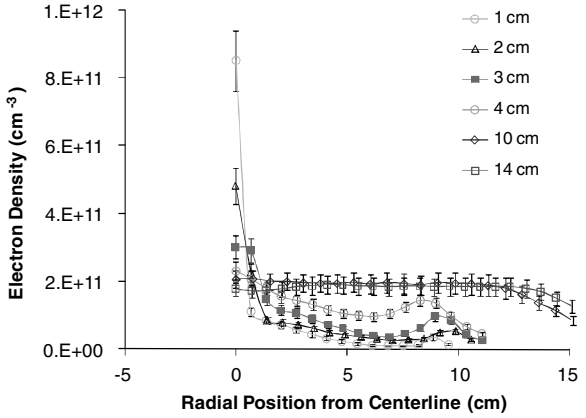

Fig. 9 Electron number density radial profiles at TH15 for the V2 configuration.

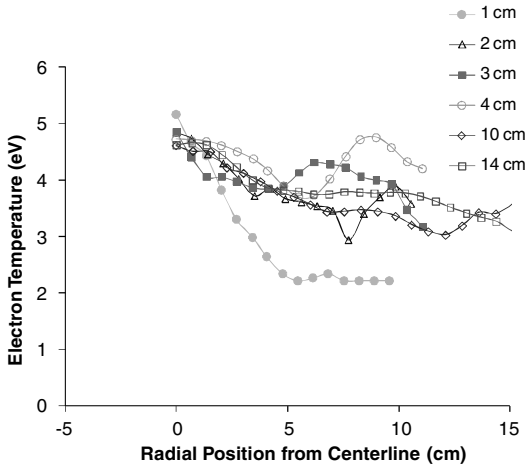

Fig. 10 Electron temperature radial profiles at TH15 for the V2 configuration. Measurement uncertainty is ±0.5 eV for all traces.

Variation in ion saturation current density was identical to electron current density. In the conical section, n_i was highly peaked on axis and also exhibited a secondary peak due to the new magnetic cusp. Ion current density in the cylindrical segment was essentially flat from the centerline out to 13 cm radially. The 14 cm probe trace, which was used as the beam profile measurement for these studies, exhibited a flatness parameter of greater than 85%, largely due to the field free volume in the cylindrical segment near the grids (as shown in Sec. V).

D. Enhanced Four-Ring Cusp: Configuration V3

1. *Overall Performance*

Configuration V3 is a four-ring-cusp modified engine. In this configuration, in addition to the conical ring added in V2, the middle magnet ring was strengthened by adding a ring of magnets to the interior of the discharge chamber, directly over the existing cylindrical section ring. The steel shim from V2 was removed from the conical ring to reduce primary electron loss to this cusp. Removal of the shim increased the cusp strength to 1800 G. Figure 11 is a plot of the magnetic contours and field lines. This configuration closed the 50 G contour throughout the chamber at the expense of reducing the field free volume in the cylindrical segment of the discharge chamber, specifically, just upstream of the optics. Primary electron loss is less than 10% in this configuration, due to the high-strength cusps, therefore all gains in performance improvement can be attributed to enhanced ion confinement (reduced ion loss to the walls) [20].

Table 6 is a performance summary of the V3 configuration. For TH15, the discharge current needed to produce 1.76 A of beam current was only 11.5 A, a 20% reduction from the nominal configuration. This resulted in a discharge loss of 167.8 eV/ion versus 207 eV/ion for the nominal NKO1 performance. Similar gains in discharge loss and total thruster efficiency were achieved for the throttled conditions as well. This indicates that increasing the gauss level of the closed magnetic contour closest to the anode serves to magnetically confine ions and reduce their loss to the walls. More detail on this mechanism will be discussed in the following sections.

2. *Plasma Profiles*

Radial plasma parameter profiles for configuration V3 were made at 1, 2, 3, 4, 10, and 14 cm axially with respect to the discharge cathode exit for the TH15 operating point. In the conical region of the discharge chamber, the radial variation in electron density had a primary peak on the centerline, with a secondary peak off axis (Fig. 12). The primary peak on the centerline had a maximum value of 4.5×10^{11} cm^{-3}, 1 cm downstream of the cathode. The secondary peak was caused by the addition of the conical magnet ring, causing electrons to travel along the field lines to the new magnetic cusp. The maximum number density in the secondary peak was

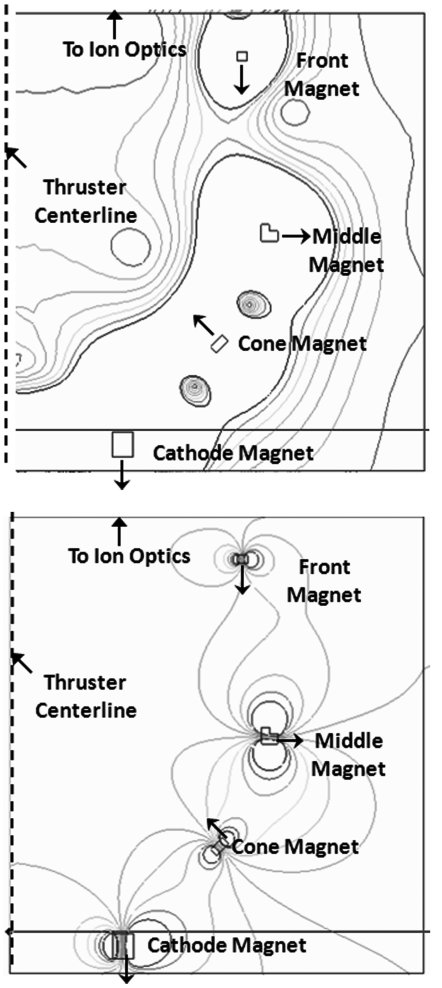

Fig. 11 Two-dimensional axis-symmetric simulation of (top) magnetic field lines and (bottom) contours of constant magnetic field of the V3 configuration. Arrows next to each magnet indicate the direction of magnetization. Thruster centerline was the axis of symmetry for the simulation.

1.75×10^{11} cm^{-3}, 4 cm radially from the centerline. Figure 13 indicates the radial variation of electron density in the cylindrical region of the plasma decreased monotonically out to the anode wall. It varied from a maximum of 2×10^{11} cm^{-3} on the centerline to 5×10^{10} cm^{-3} near the anode wall. The radial variation of T_e in the conical segment was peaked on axis (4.5 eV), with an additional off-axis peak (3 eV) corresponding to the electron density peaks described previously. T_e reached a minimum of 2 eV in the conical section, radially in from the secondary peak, suggesting that both primary and secondary electrons were tightly confined to the field lines terminating at the magnetic cusps. Radial variation in the cylindrical segment was less peaked and spanned 4–2.5 eV, with the maximum on the centerline and minimum at the anode wall. Figure 14 indicates the V_p structure in both the conical and cylindrical region of the discharge chamber exhibited a radial trend of increasing potential with proximity to the anode wall. In the

Table 6 Four-ring cusp V3 performance

Discharge parameter	NKO (V3) TH15	TH8	TH0
J_B, A	1.76	1.10	0.51
J_D, V	11.5	7.3	4.3
V_D, V	25.6	26.5	25
ε_b, V	167.8	176.4	211.4
η_{tot}	0.628	0.613	0.415

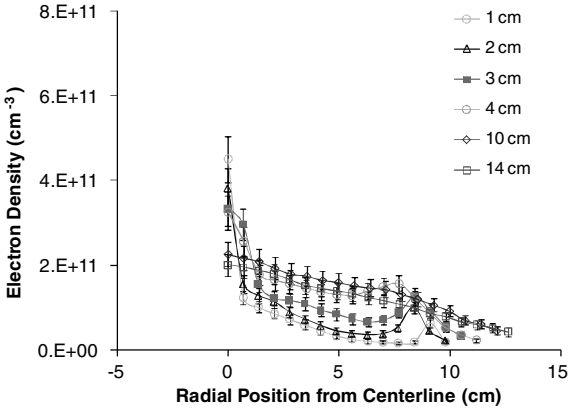

Fig. 12 Electron number density radial profiles at TH15 for the V3 configuration.

conical section, the V_p was roughly 26 V on axis and increased up to 32 V near the anode wall. In the cylindrical region of the chamber, the radial variation was relatively flat from the centerline out to 11 cm. From 11 cm to the anode wall, however, the potential increased by 2–3 V.

Although not shown, ion current density was highly peaked on axis, with a secondary peak off axis due to the new magnetic cusp. This behavior is consistent with the electron current density, indicating that the electrons electrostatically confine the ions and quasi neutrality is maintained throughout the plasma. In the near-grid (cylindrical) region, ion current density was peaked on the centerline and exhibited a monotonically decreasing radial profile out to the anode. This behavior is markedly different than configuration V2, which had a uniform radial plasma profile. The increased magnetic field strength in this configuration reduced the field free region, which tends to make the plasma less uniform as it is more constrained.

E. Enhanced Three-Ring-Cusp NASA Solar Electric Propulsion Application Readiness: Configuration V4

1. Overall Performance

Configuration V4 is an enhanced three-ring-cusp engine. In this configuration, the conical ring from V3 was removed and the strengthened middle magnet ring was left in place. The cathode magnet ring polarity was reversed to allow for alternating polarity magnetic cusps. This configuration also closed the 50 G contour throughout the chamber. The removal of the conical ring increased the field free volume throughout the chamber and depressed the field line in the cylindrical segment, as compared with V3 (Fig. 15). This configuration separates the effects of increasing the closed contour line strength inside the chamber versus adding another cusp to drive primary electrons off axis.

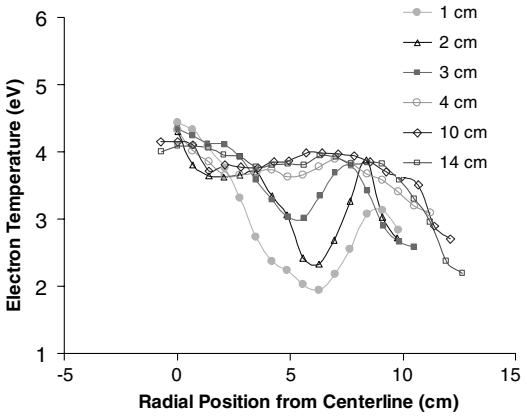

Fig. 13 Electron temperature radial profiles at TH15 for the V3 configuration. Measurement uncertainty is ±0.5 eV.

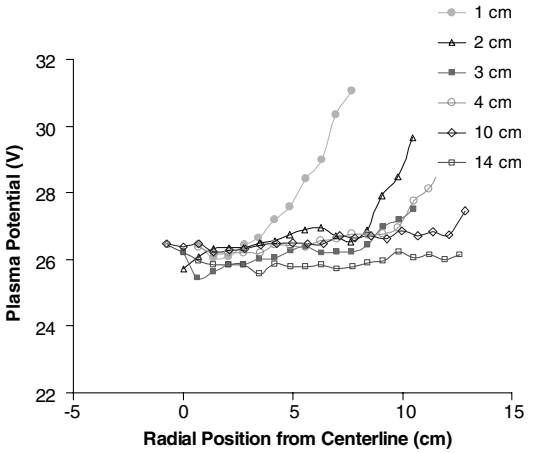

Fig. 14 Plasma potential radial profiles at TH15 for the V3 configuration. Measurement uncertainty is ±0.5 eV.

Table 7 is a performance summary of the V4 configuration. For TH15, the discharge current needed to produce 1.76 A of beam current was 11.6 A, as compared with 11.3 A for V2 and 14.5 A for V1. The discharge loss for V4 was 165 eV/ion, a 21% reduction from the nominal NSTAR configuration. Similar gains in discharge loss and total thruster efficiency were achieved for the throttled conditions as well, with a 10 and 19% reduction in discharge loss at TH8 and TH0 operation, respectively.

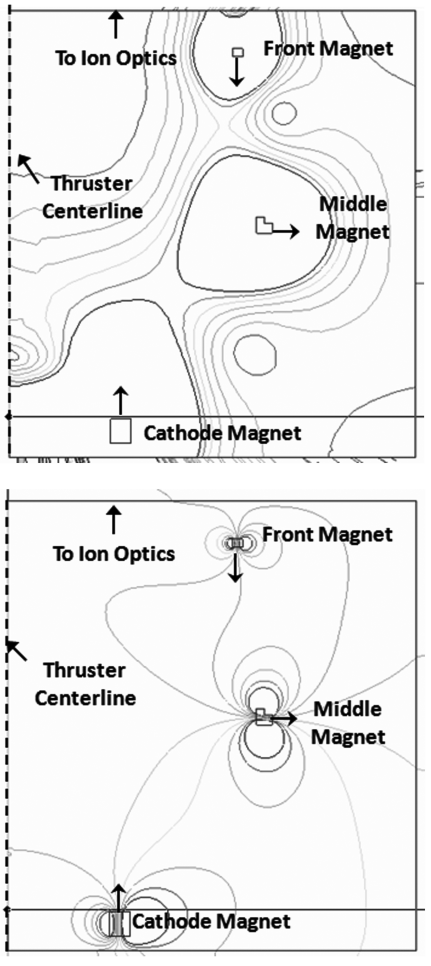

Fig. 15 Two-dimensional axis-symmetric simulation of (top) magnetic field lines and (bottom) contours of constant magnetic field of the V4 configuration. Arrows next to each magnet indicate the direction of magnetization. Thruster centerline was the axis of symmetry for the simulation.

Table 7 Enhanced three-ring-cusp V4 performance

Discharge parameter	NKO (V4) TH15	TH8	TH0
J_B, A	1.76	1.1	0.51
J_D, V	11.6	7.5	4.5
V_D, V	25.1	26.2	24.65
ε_b, V	166.3	179.1	218.1
η_{tot}	0.629	0.612	0.396

2. Plasma Profiles

Radial plasma parameter profiles for configuration V4 were made with six flat-disk langmuir probes located at 1, 2, 3, 6, 10, and 14 cm axially with respect to the discharge cathode exit. Figures 16 and 17 are plots of n_e and T_e. In the conical region of the discharge chamber, the radial variation in electron density was highly peaked on the centerline. It reached a maximum value of 1.1×10^{12} cm^{-3}, as measured 1 cm downstream of the cathode on axis and a minimum of 3×10^{9} cm^{-3} at the anode wall in the conical segment. It is important to note that this radial profile has the same axial peak value as the nominal configuration but a significantly lower density off the centerline. Therefore, the radial averaged n_e is proportionately lower for configuration V4, consistent with the discharge current set point. The radial variation of electron density in the cylindrical region of the plasma was relatively flat, from the centerline out to 10 cm radially, at 2×10^{11} cm^{-3}. From 10 to 15 cm radially, the electron density decreased monotonically from 2×10^{11} cm^{-3} to 1×10^{9} cm^{-3} near the anode wall. Error bars are not shown on the figure for clarity. The radial variation of T_e in the conical segment was peaked on axis (4.9 eV) and decreased monotonically to a minimum of 2.3 eV near the anode wall. Variation in the cylindrical segment was less peaked and spanned 4.0–3.3 eV, from the centerline out to 11 cm radially. From 11 cm to the anode wall, T_e decreased monotonically to a minimum of 2.4 eV. The V_p structure in the conical region of the discharge chamber decreased with axial distance from the cathode by approximately 1 V. As in configuration V3, the V_p increased with radial distance from the centerline, from 23 V on the centerline to 26 V near the anode wall. In the cylindrical region of the chamber, the V_p was peaked on axis, but exhibited little radial variation outside of the cathode plume region out to 12 cm radially.

In the conical section, ion current density was highly peaked on axis, but became less peaked with axial distance from the cathode (as shown later). In the near-grid (cylindrical) region, n_i was flat from the centerline out to 11 cm radially. From 11 to 15 cm, the ion current density decreased monotonically to the anode wall (Fig. 18). This behavior is different than V3, which had a nonuniform beam profile from the centerline to the anode wall.

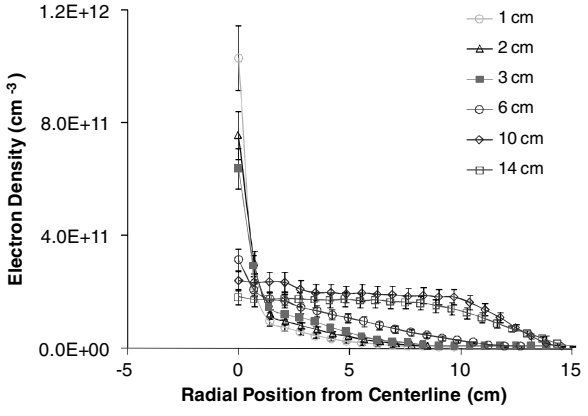

Fig. 16 Electron number density radial profiles for theV4 configuration.

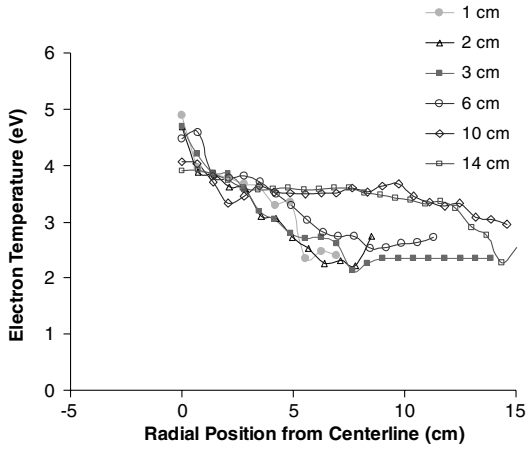

Fig. 17 Electron temperature radial profiles for the V4 configuration. Measurement uncertainty is ±0.5 eV.

V. Discussion

A. Plasma Parameters

The plasma parameter measurements for the nominal configuration (V1) indicated that the plasma density and temperature are peaked on axis, consistent with increased ionization on the centerline due to primaries emanating from the discharge cathode. This results in a radially nonuniform plasma and is consistent with faraday probe traces taken in [6]. The plasma parameter measurements for the V2 four-ring-cusp configuration indicated that the electron density, ion current density, and temperature had a primary peak on axis, as well as a secondary peak off axis in the vicinity of the new magnetic cusp. The addition of the new cusp brought primary electrons and ions off of the centerline and created a more radially uniform plasma throughout the chamber as compared with the nominal configuration. The V2 configuration yielded a remarkably flat ion current density profile just upstream of the optics, which represents the optimum profile for an ion thruster in terms of minimizing grid wear [8] and thrust vector losses. The plasma parameter measurements for the V3 four-ring-cusp configuration also indicated that the electron density, ion current density, and temperature had a primary peak on axis, as well as a significant secondary peak off axis in the vicinity of the conical segment magnetic cusp. The addition of the conical cusp brought electrons and ions off of the centerline and improved plasma uniformity in the cylindrical section. The addition of the strengthened middle magnet ring increased ion confinement, resulting in a 20% decrease in discharge loss from the nominal configuration. The strengthening of the middle magnet ring reduced the magnetic field free region in the cylindrical section, and this resulted in a peaked ion current density profile just upstream of the

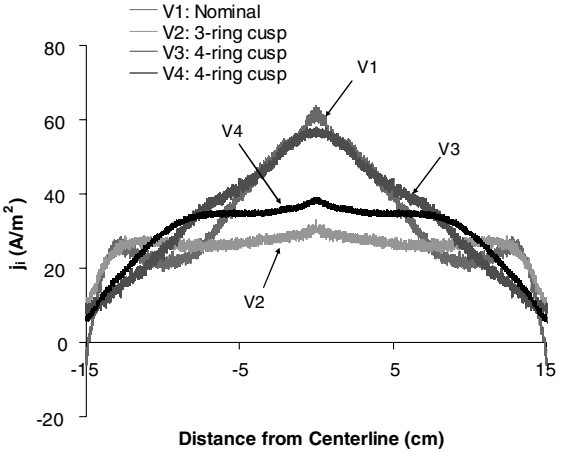

Fig. 18 Ion current density comparison for 14 cm downstream of cathode (near-grid region) showing mirror image of data from 0 to −15 cm. Measurement uncertainty is 0.4 A/m^2.

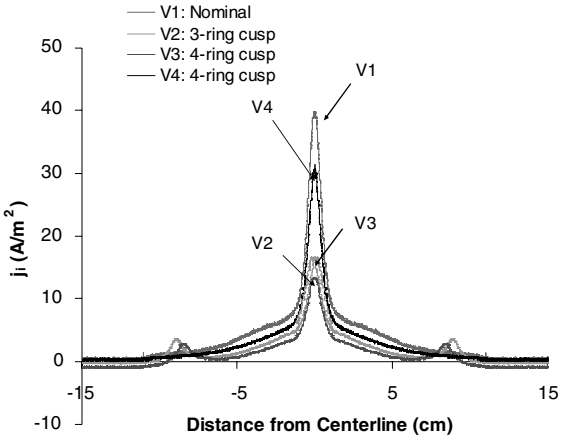

Fig. 19 Ion current density comparison for 2 cm downstream of cathode showing mirror image of data from 0 to −15 cm. Measurement uncertainty is 0.4 A/m^2.

optics similar in magnitude to the nominal configuration. The plasma parameter measurements for the V4 three-ring-cusp configuration indicated that the electron density, ion current density, and temperature had a large primary peak on axis and nonuniform plasma in the conical region of the discharge chamber. In the cylindrical region, the plasma was uniform and exhibited a 90% flatness parameter just upstream of the screen grid. This is consistent with the primary and secondary electrons brought off axis in their transit to the strengthened middle magnet ring. The ion current density profiles also show a significant flattening out, suggesting that ions are electrostatically confined to the electrons. Configuration V4 also had a 20% reduction in discharge loss as compared with the nominal configuration. The strengthening of the middle magnet ring without an additional conical cusp increased the magnetic field free region in the cylindrical section, resulting in a flat ion current density profile from the centerline out to 11 cm.

B. Plasma Uniformity

An important finding of this study is that improving plasma uniformity in the conical region is not a requirement for improving the plasma uniformity in the near-grid region. Figure 18 shows the beam profiles, that is, scans that were taken 14 cm downstream of the cathode. The mirror image of the data is plotted on the graph to show what the entire beam profiles would look like. Configuration V2 has a flat beam profile versus V3 which is peaked on axis. Figure 19 is ion current density taken at 2 cm downstream of the cathode. Here, V3 has the flattest beam profile and V4 the most peaked. Configuration V3, which had the most uniform conical region plasma, had the least radially uniform plasma profile in the near-grid (cylindrical) region. Therefore, driving primary electrons off axis to an additional conical cusp is not required to flatten the near-grid beam profile. Plasma uniformity in the near-grid region is dependent on the local magnetic field structure. It is an increase in the field free volume of the cylindrical region that is critical for producing a flat beam profile.

C. Discharge Chamber Physics

To understand the mechanisms that define the discharge chamber plasma, examination of the electron population is required. As electrons are light, their motion is governed by electron cyclotron gyration about the field lines as they drift toward the magnetic cusps. Ions will follow electrons in their magnetically constrained motion to shield out electric potentials that would otherwise exist due to electron magnetic confinement. The electron population in the discharge plasma is approximately 90% Maxwellian electrons and 10% primary electrons from the cathode [3]. The primary electrons, with energy at approximately the discharge voltage, are well confined by the magnetic multicusp field, with 90% of the primary population having an inelastic collision and only 10% being lost to the magnetic cusps for the nominal configuration [3]. These inelastic collisions form the Maxwellian or secondary electron population with a Gaussian energy distribution defined by the electron temperature. At only 4–5 eV, if not adequately magnetically constrained, secondary electrons can radially diffuse to the anode walls or diffuse rapidly to the magnetic cusps. Radial diffusion can be represented by random walk of the charged particle in the direction opposite the density gradient [21]. For random walk across a magnetic field, as is the case in an ion thruster, the diffusive path length or average distance between collisions is defined by the Larmor radius. Therefore, minimizing electron diffusion is a function of the magnetic field strength. As ions are electrostatically retarded/attracted by the electrons, the ions will also be confined. The V_p profiles for the cases investigated support this theory. In the cases where ion confinement was enhanced, the V_p near the anode wall increased in value, suggesting electron loss to the walls was impeded and ion motion to the wall retarded. Conversely, in the cases where ion confinement was poor, there was no radial gradient in potential in the anode wall region, allowing the ions to diffuse out radially. The measurements do not provide quantitative insight into whether diffusion in the presence of the ring-cusp magnetic field is purely radial or purely along the field lines to magnetic cusps. It is likely that primary electrons diffuse only along the magnetic field lines, due to their small Larmor radius. Electron density measurements also confirm that the bulk Maxwellian electron population is also constrained by the field lines on their way to the cusp. In either case, constraining more electrons to the field lines by reducing their Larmor radius will also minimize ion diffusion to the wall, due to the requirement that the total diffusion must be ambipolar.

D. Lifetime Implications

In addition to the performance and total efficiency improvement obtained by reducing the discharge loss by 20%, there are lifetime enhancements for the NSTAR thruster. Hollow-cathode emitter life is a function of the insert temperature, which depends exponentially on the current density [1]. Using the depletion rate coefficients developed by Palluel and Shroff [22], operation at 11.3 A versus 14.5 A, increases cathode life, from the perspective of barium depletion, by up to 45% for TH15 operation [10]. Similarly, reducing the peak current density by flattening out the beam profile can significantly increase grid life over the nominal configuration. The grid erosion rate is linearly dependent on current density, therefore a 20% reduction in peak beam current density could increase grid life by as much as 20% [10].

VI. Conclusions

It has been shown experimentally that improving ion confinement is the key mechanism for improving the electrical efficiency of the NSTAR thruster. In cases V3 and V4, which operated at roughly 11.5 A of discharge current versus 14.5 A for the nominal configuration, the radially averaged n_e was proportionately lower than the nominal configuration, but the extracted beam current was identical for all configurations. In the nominal configuration, more ions were created due to the higher discharge current operation, but more were lost to recombination with the walls as compared with the enhanced configurations.

Another key finding is that plasma uniformity in the conical region does not necessarily improve the plasma uniformity in the near-grid region. In the case of V3, the addition of a conical cusp reduced near-grid uniformity by reducing the field free volume in the discharge chamber. It is therefore the near-grid magnetic structure that defines the beam profile. However, depending on the size of the discharge chamber, conical cusps may need to be added to close a sufficiently high gauss contour line to prevent ion loss. However, the cusps should be situated so as to maximize the field free volume of the plasma.

The spatially resolved experimental measurements have provided a quantitative understanding of the confinement and production of the discharge plasma. The experimental investigations have mapped out the plasma structure and its confinement as a function of the magnetic

field parameters. The new engine configurations investigated have experimentally demonstrated magnetic field configurations that improve ionization efficiency and plasma uniformity. The enhancements in efficiency and cathode and grid lifetime were accomplished via straightforward changes in the magnetic field, leaving the possibility for further optimization wide open.

Acknowledgments

The authors would like to acknowledge Dennis Fitzgerald and Ray Swindlehurst of the Jet Propulsion Laboratory, who assisted in the preparation and conduct of this research. The Jet Propulsion Laboratory, California Institute of Technology carried out the research described in this paper, under a contract with NASA.

References

[1] Randolph, T., "Qualification of Commercial Electric Propulsion Systems for Deep Space Missions," *The 30th International Electric Propulsion Conference*, Electric Rocket Propulsion Society, IEPC Paper 2007-271, 2007.

[2] Oh, D. O., "Evaluation of Solar Electric Propulsion Technologies for Discovery Class Missions," *The 41st AIAA/ASME/SAE/ASEE Joint Propulsion Conference and Exhibit*, AIAA Paper 2005-4270, 2005.

[3] Goebel, D. M., Wirz, R., and Katz, I., "Analytical Ion Thruster Discharge Performance Model," *Journal of Propulsion and Power*, Vol. 23, No. 5, 2007, pp. 1055–1067. doi:10.2514/1.26404

[4] Wirz, R., "2D Discharge Chamber Model for Ion Thrusters," *The 40th Joint Propulsion Conference*, AIAA Paper 2004-4107, July 2004.

[5] Goebel, D. M., Watkins, R. M., and Jameson, K. K., "LaB_6 Hollow Cathodes for Ion and Hall Thrusters," *Journal of Propulsion and Power*, Vol. 23, No. 3, May–June 2007, pp. 552–558. doi:10.2514/1.25475

[6] Sengupta, A., Brophy, J. R., Anderson, J. A., Kulleck, J., de Groh, K., Banks, B., and Karniotis, T.,"The 30,000-Hr Life Test of the DS1 Flight Spare Ion Thruster, Final Report," NASA TP 2004-213391, 2004.

[7] Mikellides, I. G., Katz, I., Goebel, D. M., and Polk, J. E., "Theoretical Model of a Hollow Cathode Plasma for the Assessment of Insert and Keeper Lifetimes," *The 41st AIAA/ASME/SAE/ASEE Joint Propulsion Conference*, AIAA Paper 05-4234, 2005.

[8] Anderson, J., Katz, I., and Goebel, D., "Numerical Simulation of Two-Grid Ion Optics Using a 3D Code," *40th Joint Propulsion Conference*, AIAA Paper 2004-3782, 2004.

[9] Sengupta, A., Goebel, D., Fitzgerald, D., Owens, A., Tynan, G., and Doerner, R., "Experimentally Determined Neutral Density and Plasma Parameters in a 30 cm Ion Engine," *40th Joint Propulsion Conference*, AIAA Paper 2004-3613, 2004.

[10] Sengupta, A., "Experimental and Analytical Investigation of a Ring Cusp Ion Thruster: Discharge Chamber Physics and Performance," Ph.D. Dissertation, Dept.of Aerospace Engineering, Univ. of Southern California, Los Angeles, 2005.

[11] Kolasinski, R. D., and Polk, J. E., "Characterization of Cathode Keeper Wear By Surface Layer Activation," *39th Joint Propulsion Conference*, AIAA Paper 2003-5144, 2003.

[12] Sengupta, A., Anderson, J. R., Garner, C., Brophy, J. R., de Groh, K., Banks, B., Karniotis, C., "Overview of the Results from the 30,000 Hr Life Test of the Deep Space 1 Flight Spare Ion Engine," *40th Joint Propulsion Conference*, AIAA Paper 2004-3608, 2004.

[13] Herman, D. A., and Gallimore, A. D., "Comparison of Discharge Plasma Parameters in a 30-cm NSTAR Type Ion Engine with and Without Beam Extraction," *39th Joint Propulsion Conference*, AIAA Paper 03-5162, 2003.

[14] Huddlestone, R. H., *Plasma Diagnostic Techniques*, Academic Press, Los Angeles, 1965, pp. 113–200.

[15] Godyak, V. A., Piejak, R. B., and Alexandrovich, B. M., "Probe Diagnostics of Non-Maxwellian Plasmas," *Journal of Applied Physics*, Vol. 73, No. 8, April 1993, pp. 3657–3663. doi:10.1063/1.352924

[16] Clements, R. M., "Plasma Diagnostics with Electric Probes," *Journal of Vacuum Science and Technology*, Vol. 15, No. 2, April 1978, p. 193. doi:10.1116/1.569453

[17] Figliola, R. S., and Beasley, D. E., *Theory and Design for Mechanical Measurement*, 2nd ed., Wiley, New York, 1995.

[18] Williams, G. J., Jr., Smith, T. B., Patrick, T. A., and Gallimore, A. D., "Characterization of the FMT-2 Discharge Cathode Plume," *26th International Electric Propulsion Conference*, Electric Rocket Propulsion Society, IEPC-99-104, Oct. 1999.

[19] Jameson, K., Goebel, D. M., and Watkins, R., "Hollow Cathode and Keeper-Region Plasma Measurements," *The 41st AIAA/ASME/SAE/ASEE Joint Propulsion Conference*, AIAA Paper 2005-3667, 2005.

[20] Sengupta, A., "Experimental and Analytical Investigation of a Modified Ring Cusp Ion Thruster," *The 29th International Electric Propulsion Conference*, Electric Rocket Propulsion Society Paper IEPC 2005-160, Oct. 2005.

[21] Chen, F. F., *Introduction to Plasma Physics and Controlled Fusion*, 2nd ed., Plenum, New York, 1984.

[22] Palluel, P., and Shroff, A. M., "Experimental Study of Impregnated Cathode Behavior, Emission, and Life," *Journal of Applied Physics*, Vol. 51, No. 5, May 1980, pp. 2894–2902. doi:10.1063/1.327959

R. Myers
Associate Editor